Case Studies in Thermal Engineering 26 (2021) 101138

Contents lists available at ScienceDirect

Case Studies in Thermal Engineering

journal homepage: www.elsevier.com/locate/csite

Physico-chemical characterization, thermal decomposition and kinetic modeling of *Digitaria sanguinalis* under nitrogen and air environments

Ayokunle O. Balogun [a], Adekunle A. Adeleke [a,*], Peter P. Ikubanni [a], Samuel O. Adegoke [b], Abdulbaset M. Alayat [c], Armando G. McDonald [c]

[a] Department of Mechanical Engineering, College of Engineering, Landmark University, Omu-Aran, Nigeria
[b] Department of Petroleum Engineering, Faculty of Engineering and Technology, University of Ibadan, Nigeria
[c] Department of Forest, Rangeland and Fire Science, University of Idaho, Moscow, ID 83844-1132, USA

HIGHLIGHTS

- Fatty acids detected ranged from C_{12} (lauric acid) to C_{24} (lignoceric acid).
- DS had fixed carbon content of 17.85% and calorific value of 13.7 MJ kg^{-1}.
- For N_2 and air, in the latter stages, different activation energy trends were noted.
- Chemical reaction and diffusional models were predominant in the decomposition.
- In air, a prominent peak protrudes at about 450 °C as against a shoulder under N_2.

GRAPHICAL ABSTRACT

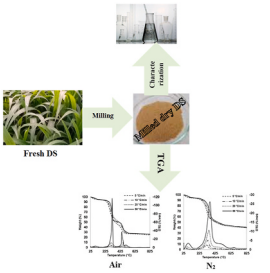

ARTICLE INFO

Keywords:
Kinetics
Model-fitting
Digitaria sanguinalis
Isoconversional
Thermogravimetry

ABSTRACT

The study undertook the thermal degradation of a tropical grass species, *Digitaria sanguinalis,* in nitrogen (pyrolysis) and air (combustion) atmospheres through thermogravimetric analysis as well as comparative kinetic investigation. The differential (Friedman) and integral (Flynn-Wall-Ozawa and Straink) isoconversional methods in conjunction with the Coats-Redfern method were utilized. This was to obtain the kinetic parameters and also predict the probable reaction mechanisms involved in the decomposition process. Before the thermal and kinetic investigations, the grass was analyzed for its physical, chemical, and structural properties utilizing diverse wet-chemistry and spectroscopic techniques. This research attempt is part of a larger project designed to investigate a couple of local grass species, which are invasive by nature, as potential energy crops for pyrolytic and combustion applications. The grass had a fixed carbon content of 17.85%

* Corresponding author.
E-mail address: adeleke.adekunle@lmu.edu.ng (A.A. Adeleke).

https://doi.org/10.1016/j.csite.2021.101138
Received 1 March 2021; Received in revised form 4 June 2021; Accepted 5 June 2021
Available online 12 June 2021

and a calorific value of 13.7 MJ kg^{-1}. The fatty acids detected were from C12 (lauric acid) to C24 (lignoceric acid), with the three most abundant being palmitic (94 mg/g extract), linoleic (27 mg/g extract), and oleic (19 mg/g extract) acids. The average residual weight in air (25.3%) was relatively less than in nitrogen (38.7%), affirming the higher rate of reaction in an oxidative process (combustion). The activation energy profiles in both atmospheres were markedly different, as shown by the Flynn-Wall-Ozawa technique for a conversion ratio of 0.1–0.2 (nitrogen, 149 kJ/mol; air, 177 kJ/mol) and 0.65–0.8 (nitrogen, 366 kJ/mol; air, 170 kJ/mol). Of all the models tested, the model-fitting technique indicates that the chemical reaction and diffusional models play predominant roles in the thermal decomposition of the grass under investigation. The thermal degradation of *Digitaria sanguinalis* proceeded mainly as complex multi-step reaction mechanisms. Aside from the potential suitability of the grass species for bioenergy applications and biofuels production, it also demonstrated huge capability for biochemical extraction. Future work will incorporate the kinetic data for the associated thermochemical processes development, and the design and optimization of reactors/combustors.

Nomenclature

Abbreviations

A	pre-frequency factor (min^{-1})
CCI	cellulose crystallinity index (−)
C	carbon content (wt%)
E_α	apparent activation energy (kJ/mol)
FC	fixed carbon (wt%)
$f(\alpha)$	integral decomposition model (−)
HHV	higher heating value (MJ/kg)
LOI	lateral order index (−)
M^+	molecular weight (m/z)
N	reaction order (−)
N	nitrogen content (wt%)
RT	retention time (min)
R	universal gas constant ($8.314 J/mol \cdot K$)
S/G	syringyl/guaiacyl ratio (−)
TCI	total crystallinity index (−)
T_p	peak temperature (°C)
T	time (min)
T	temperature (K)
VM	volatile matter content (wt%)
W	weight at temperature T (%)
W_i	initial weight (%)
W_f	residual weight (%)
$wt\%$	weight percentage

Greek Symbols

α	conversion ratio (−)
B	heating rate (°C/min)

Latin Symbols

Ø	diameter

1. Introduction

An attempt to mitigate the adverse effects of global warming and climate change occasioned by overdependence on fossil fuel has led to an insatiable quest for alternative and renewable energy resources [1,2]. Lignocellulosic biomass is a critical resource in the renewable energy spectrum because it is carbon neutral, abundantly available as residues, and has a wide geographical reach. A variety of biomass types which includes agricultural residues [3], woody materials [4], algae, and municipal solid wastes [5], have been explored as feedstock materials for bioenergy production. Of recent, however, researchers have shown keen interest in studying some grass species for bioenergy and biofuels applications because of their short growth duration, ease of harvest and processing, low

maintenance requirement, and significant contribution to CO_2 emission reduction [6].

Digitaria sanguinalis (DS), also known as crabgrass, is an important grass that belongs to the Poaceae family [7]. DS undergoes an annual growth cycle and has been reported to be prolific in seed-bearing and reproduction [8]. In addition, it thrives well in both the temperate and tropical regions; though, it is regarded as an invasive weed that competes for water, air, and nutrients. Generally, grasses could be supported by varied weather conditions, low-fertility soil, and low-water requirements. It is also noteworthy that DS is a C_4 plant that has a particular advantage of absorbing CO_2 and converting solar energy to chemical energy through the C_4 photosynthesis pathway [6]. This is the most efficient pathway to photosynthesis because it maximizes CO_2 fixation. Thus, facilitating the production of organic compounds in lignocellulosic biomass. The cultivation of DS would promote the reversal of global warming through its carbon sequestration prospect. Hidayat et al. [6] observed that an efficient CO_2 fixation is a vital factor in choosing an energy crop. Despite the promises that DS holds, the exploration of grasses for biofuels applications is still in its infancy. With the prolific and invasive nature of grasses, this study is part of a larger research endeavor to investigate the suitability of some local grass species as a potential feedstock for thermochemical conversion processes.

The recalcitrant nature of lignocellulosic biomass makes them more amenable to thermochemical conversion techniques. As a result, the thermal means (e.g., combustion [9], torrefaction [10], and pyrolysis [6]) have become the most prominent in the bioenergy sector. The commonest means are pyrolysis [4,6], which occurs in an oxygen-lean environment, and combustion [9,11], which is essentially an oxidizing process. Most often, pyrolysis is used for the extraction of chemicals and biofuels such as syngas, bio-oil, and biochar. Syngas and bio-oil can be deployed for energy recovery because of their relatively high heating values, while bio-oil can be processed into transportation fuels and other biochemical products [12]. Biochar can be used for soil amendment and purification purposes, as well as fuel [12]. Furthermore, lignocellulosic biomass is often subjected to combustion or co-firing for electricity generation and heat recovery purposes [13]. Though the early stages of pyrolysis and combustion processes have similar characteristics, each process still follows different chemical reaction pathways; and decomposition mechanisms – leading to distinct reaction kinetics. Wu et al. [12] studied the kinetics and reaction chemistry of the pyrolysis and combustion of tobacco waste in TGA experiments at five different heating rates. They observed distinctive reaction mechanisms for both processes. They reported that, though the first stage of both processes was similar, pyrolysis had one additional decomposition stage. The study concluded that the effective activation energies for the combustion process was relatively lower. Mlonka-Mędrala et al. [14] investigated the effect of biomass particle size on the pyrolysis and combustion of three different lignocellulosic biomass resources in a TG GC/MS analysis. They concluded that particle size variation influences the activation energy significantly during combustion but marginally during pyrolysis. A comparative study was conducted to examine the combustion and pyrolysis behaviors of peanut shells in air and nitrogen through a TG/DSC analysis. It was observed that the thermal performance parameters were comparatively higher in the air experiment [15]. They also noted that the temperature that represents the end of the reaction varies significantly for both atmospheres.

A heterogeneous lignocellulosic biomass feedstock consists of a complex matrix of low-molecular organics, macromolecular polymers, and inorganics [16,17]. The origin, species, and feedstock type determine the biomass structure and composition, which influences the biomass thermal decomposition and the subsequent char formation and volatile release. According to Hidayat et al. [6], grass plants consist of loosely bound fibers with a lower proportion of lignin components relative to woody resources. Apparently, this has the capacity to influence the decomposition pathway and product yields during thermal decomposition processes. Concerning the effects biomass composition on decomposition kinetics, it was shown that among Miscanthus, acacia, and pine samples, *Miscanthus giganteus*, a grass species, had the highest activation energy [13]. This was attributed partly to the temperature dependence of the chemical and pore structure variation [13]. Karampinis et al. [18], in a comparative thermal study of Greek lignite and five different energy crops, namely, cardoon, *Miscanthus*, *Paulownia*, willow, and poplar, observed significant variations in the values of the activation energy for the respective polymeric constituents. They also concluded that *Miscanthus* and other wood samples had a relatively higher char reactivity. The bulk of the bioenergy-related investigation done on different grass species focused on their physico-chemical and structural characterization [6,19]. There are limited attempts at undertaking comparative kinetics modeling and the thermal decomposition of grass species in air and inert atmospheres. It is essential to understand the decomposition process to achieve efficient reactor design and successfully undertake the modeling and optimization of the associated thermal processes. Again, the kinetic data could be incorporated as sub-models in transport phenomena investigation for a much larger scale project.

It is vital to combine experimental analyses with modeling to understand decomposition mechanisms and reaction kinetics. Biomass decomposition processes are often captured by kinetic modeling; particularly, when it involves negligible thermal gradient effects and slow heating rates. Kinetic models are reputed for their simplicity and strong predictive capability. Furthermore, they are fitted to thermogravimetric analysis (TGA) data for the evaluation of the kinetic parameters, which are subsequently utilized for simulation. The mathematical procedure employed in obtaining solutions requires two essential techniques - model-free (isoconversional) and model fitting. In the model-free technique, the knowledge of the reaction mechanism is not necessary and obviates the need for the decomposition model in the rate equation. Though it relatively simplifies kinetic analysis, it excludes information on the reaction scheme. It also requires multiple TGA measurements at different heating rates. Lopes et al. [20] undertook the kinetic investigation of guarana seed residue using an iso-conversional method and affirmed that activation energy varied with conversion in both pyrolytic and oxidizing environments. Onsree et al. [4] studied the pyrolysis behavior and kinetics of corn residue pellets and eucalyptus wood chips in a macro TGA deploying an integral model-free algorithm of FWO. They noted that the activation energy obtained was about four times lower than those in a typical TGA experiment. Balogun et al. [21] investigated the kinetics of the thermal decomposition of brewer's spent grains utilizing the model-free techniques and concluded that it proceeded as a multi-step mechanism process. On the other hand, the model-fitting method requires foreknowledge of the reaction mechanism to obtain a precise decomposition model. In this case, the kinetic parameters are evaluated by choosing a model of best-fit from a couple of decomposition models fitted to TGA data. The major merit is that the reaction model choice gives an understanding of the possible

decomposition mechanism. A commonly utilized model-fitting method is Coats-Redfern (CR) integral technique. Almazrouei and Janajreh [22] deployed two model-fitting approaches, namely, direct differential and CR methods, to deduce the non-isothermal kinetic parameters of the pyrolysis of pure and crude glycerol. The techniques present distinctive activation energy values for the samples under investigation. Masnadi et al. [23] analyzed the kinetics of solid fuel pyrolysis using CR technique and concluded that the model identified the probable reaction mechanisms and activation energy values at different pyrolysis stages.

Relatively, the exploration of different grass species for bioenergy purposes is in its early days, particularly in Nigeria, and this is one of such attempts. Again, much of the thermal degradation studies have focused on either pyrolysis [4,6] or combustion [9,11] of varied biomass residues. There is still scarce research efforts in comparing the thermal behavior of biomass residues in pyrolytic and oxidizing environment [12]; in fact, much less have been explored for tropical grass species [13]. Furthermore, there is limited study that compares the kinetic analysis of biomass thermal decomposition based on model-fitting and model-free methods. Therefore, the primary objective of this study was to conduct the thermal decomposition of a tropical grass, DS, and undertake its kinetic analysis through a model-fitting and an isoconversional approach. The DS sample was characterized through proximate and ultimate analyses, Fourier Transform Infra-Red Spectroscopy (FTIR), and X-ray diffraction (XRD). In addition, it was thermally degraded through thermogravimetric experiments under N_2 (pyrolysis) and air (combustion) environments.

2. Material and methods

2.1. Materials

The DS grass was obtained in an open field (8°7′14″N; 5°4′56″E) within Landmark University premises in June 2020. Initially, the grass was air-dried for 2 weeks. After, it was oven-dried at 70 °C for 24 h for ease of pulverization. The sample was ground in a ball mill and sieved into particle sizes ranging between 0.6 and 1.18 mm using a mechanical sieve. The 0.6 mm screened particles were used for characterization and TGA.

2.2. Biomass characterization

A Parr oxygen bomb calorimeter (model 1261) was used to obtain the HHV of compressed DS (1.0 g, 6 mm Ø using a Carver laboratory press at 68 MPa) in accordance with ASTM D5865-04. The DS ash, VM, and FC contents were determined by proximate analysis according to ASTM E870-82. The elemental analysis was performed on a Costech ESC 4010 instrument to obtain C and N contents.

The DS sample (4.0 g) was Soxhlet extracted using CH_2Cl_2 (150 mL) for 16 h, and the extractives content was determined gravimetrically, according to ASTM D1108-96. The extract was analyzed for lipid profiles as fatty acid methyl ester (FAME) derivatives after acidic methanolysis [2 mL of $CH_3OH/H_2SO_4/CHCl_3$ (1.7:0.3:2.0 v/v/v) at 90 °C for 90 min]. This was followed by gas chromatography-mass spectrometry (Thermoscientific ISQ-Trace1300; Phenomenex ZB5 30 m × 0.25 mm column; 40 °C (1 min) to 280 °C at 5 °C min^{-1}) analysis [24]. The extractive-free DS (200 mg) was analyzed for lignin and carbohydrate contents by hydrolysis in H_2SO_4 (2 mL, 72%) for 60 min at 30 °C, followed by secondary hydrolysis (4% H_2SO_4, 30 min, 121 °C) in an autoclave (ASTM D 1106–96). The Klason lignin content was determined gravimetrically after filtration. The acid soluble lignin was determined at 205 nm of the filtered hydrolysate (250 mL) using an extinction coefficient of 110 L g^{-1} cm^{-1} (Genesys 50, Thermoscientific). The carbohydrate analysis was performed on the hydrolysis filtrate (5 mL) according to ASTM E 1758-01. The monosaccharides were quantified by HPLC (two Rezex RPM columns, 7.8 mm × 300 mm, Phenomenex) at 85 °C on elution with water (0.5 mL min^{-1}) using differential refractive index detection (Waters model 2414). All analyses were performed in duplicate.

The FTIR spectroscopy was performed on an iS5 spectrometer (ThermoNicolet) in the single bounce attenuated total reflection (ATR) mode (iD5, ZnSe). The lignin S/G ratio was determined from the relative band intensities at 1462 and 1508 cm^{-1}. The cellulose crystallinity in terms of TCI was calculated from the relative band intensities at 1430 and 897 cm^{-1} [25]. The cellulose LOI was determined from the band intensity ratios at 1430 and 897 cm^{-1} [25]. The XRD was done on a Siemens D5000 diffractometer (2θ from 5 to 50° with steps of 0.2°). The diffractogram was peak fitted using Origin software before the determination of the CCI = 1 – (I_{am}/I_{002}), where I_{am} is the intensity of the peak at 2θ = 15° and I_{002} is the maximum intensity of the (002) plane diffraction at 2θ = 22°) [21].

2.3. Thermal decomposition through TGA

A biomass sample with an initial mass of 5.4 ± 0.29 mg was subjected to heating measurements in a PerkinElmer TGA-7 instrument under N_2 and dry air atmospheres at a flow rate of 30 mL min^{-1}. The heating temperature was ramped up from ambient conditions (28.9 ± 0.92 °C) to 900 °C at different heating rates (5, 10, 20, and 50 °C min^{-1}), and the data obtained were analyzed using the Pyris v11 software.

2.4. Kinetic modeling

A one-step global kinetic model for solid-state decomposition in an isothermal condition is expressed as a rate equation (Eq. (1)) [4].

$$\frac{d\alpha}{dt} = A exp^{\left(-\frac{E_\alpha}{RT}\right)} f(\alpha) \tag{1}$$

while the conversion degree is given as Eq. (2) [26].

$$\alpha = \frac{W - W_i}{W_f - W_i} \tag{2}$$

At constant linear heating rate, $\beta = dT/dt$, therefore for dynamic heating condition, Eq. (1) yields Eq. (3) [4].

$$\frac{d\alpha}{dT} = \frac{A}{\beta} exp^{\left(-\frac{E_\alpha}{RT}\right)} f(\alpha) \tag{3}$$

2.4.1. Coats-Redfern method

The temperature-rate differential equation in Eq. (3) can be integrated by separation of variables to obtain a temperature integral function (Eq. (4)) [27], which is not amenable to an analytical solution.

$$g(\alpha) = \int_0^\alpha \frac{d\alpha}{f(\alpha)} = \int_{T_0}^{T} \frac{A}{\beta} exp^{\left(-\frac{E}{RT}\right)} dT \tag{4}$$

Eq. (4) reflects the reaction mechanism associated with the solid-state decomposition and a number of such models is presented in Table 1. The logarithmic transformation of Eq. (3) alongside Eq. (4) gives the popular CR model for the determination of the kinetic parameters, as shown in Eq. (5) [11].

$$\ln\left(\frac{g(\alpha)}{T^2}\right) = \ln\frac{AR}{\beta E}\left(1 - 2\frac{RT}{E}\right) - \frac{E}{RT} \tag{5}$$

The plot of the left-hand side of Eq. (5) against the reciprocal of temperature yields approximately a linear curve from whose slope the activation energy can be deduced. It is assumed that $RT \ll E$; therefore, the pre-frequency factor can be evaluated from the intercept $\left(intercept = \ln\frac{AR}{\beta E}\right)$.

2.4.2. Differential Friedman (DFM) method

If the natural logarithm of Eq. (3) is taken, it yields Eq. (6), which is popularly referred to as differential Friedman's kinetic model [29,30].

$$\ln\left[\frac{d\alpha}{dt}\right] = \ln\left[\beta\left(\frac{d\alpha}{dT}\right)\right] = \ln[Af(\alpha)] - \frac{E}{RT} \tag{6}$$

In Friedman's relation the conversion function, $f(\alpha)$, is assumed constant. This implies that the solid-state decomposition is essentially dependent on the mass loss rate and independent of the temperature. The linear plot of $\ln\left[\frac{d\alpha}{dt}\right]$ against $\frac{1}{T}$ is generated for

Table 1
Empirical correlations for $g(\alpha)$ on different reaction mechanisms [11,28].

Mechanism model	$g(\alpha)$
Power law (n = 1, 2, 3)	$\alpha^{1/n}$
Nucleation reaction models	
Avarami-Eroféve (n = 1.5, 2, 3)	$[-\ln(1-\alpha)]^{1/n}$
Contracting sphere	$1-(1-\alpha)^{1/2}$
Contracting cylinder	$1-(1-\alpha)^{1/3}$
Diffusional models	
1-D diffusion	α^2
2-D diffusion	$[(1-\alpha)\times\ln(1-\alpha)]+\alpha$
3-D diffusion-Jander	$[1-(1-\alpha)^{1/3}]^2$
3-D diffusion-GB	$1-\frac{2\alpha}{3}-(1-\alpha)^{2/3}$
Chemical reaction models	
1st order	$-\ln(1-\alpha)$
n-th order	$[1-(1-\alpha)^{1-n}]/(1-n)$

different heating rates and the activation energy is determined from the slope $\left(slope = -\frac{E}{R}\right)$. It is important to note that the use of the derivative conversion data makes DFM prone to noise sensitivity and numerical instability. Therefore, caution must be exercised in the data interpretation [28].

2.4.3. Flynn-Wall-Ozawa (FWO) method

The FWO model takes the apparent activation energy to be constant during the thermal decomposition process and engages Doyle's relation to approximate the temperature integral function. Taking logarithm of the integral function and inserting Doyle's approximation yields Eq. (7) [24,30].

$$\log \beta = \log\left(A\frac{E}{Rg(\alpha)}\right) - 2.315 - 0.4567\frac{E}{RT} \tag{7}$$

A plot of $\log \beta$ against $\frac{1}{T}$ for different heating rates produces straight lines. Again, the activation energy can be evaluated from the slope of the lines as $\left(slope = -0.4567\frac{E}{R}\right)$.

2.4.4. Starink (STK) method

The Starink method is based on the optimization of two isoconversional methods; namely, FWO and KAS, and it is expressed as Eq. (8) [31].

$$\ln\left(\frac{\beta}{T^{1.92}}\right) = C_s - 1.0008\frac{E}{RT} \tag{8}$$

A plot of $\ln\left(\frac{\beta}{T^{1.92}}\right)$ against the reciprocal of temperature generates linear curves and the activation energy can be computed from their slopes. It was noted that the Starink's model presented an accuracy of an order of magnitude higher than the FWO and KAS.

3. Results and discussion

3.1. Characterization of DS

The results of the elemental, proximate, ultimate (ash, extractives, lignin, and carbohydrate), and calorific value analyses of DS, are given in Table 2. The DS sample contained 34% C, 2.5% N, and 4.4% ash. These elemental results are clearly in the range for lignocellulosic biomass materials. The ash content was 45% lower than that reported by Sultan et al. [32]. An estimated protein content of 15.6% was obtained and was higher than that reported by Sultan et al. [32] and Lee and Lee [33]. A FC value of 17.85% obtained from this study was found comparable to the values reported for Napier grass [34]. The HHV value obtained for DS was 13.7 MJ kg^{-1}, and it is about 25% lower than that published by Lee and Lee [33]. An extractives (lipid) content of 1.7% was obtained and in the range (1.0–3.8%) for grasses [35]. Klason lignin content of 14.2% was noted and slightly higher than what was reported in literature for DS (8.3–13.9%) [33]. The Klason and acid-soluble lignin contents were comparable to that of Napier grass [36]. The detailed carbohydrate analysis showed mainly glucan (43.6%) and xylan (20.1%) together with arabinan and galactan. The total carbohydrate value (hemicellulose + cellulose) agrees with data from existing literature [33]. Some of the variations observed in some parameter values may be due to differences in the climatic, geographical, agricultural practices, and soil nutrient availability.

Table 2
Proximate, ultimate and calorific value analyses of *Digitaria sanguinalis*.

Parameter	DS
VM (wt%)	71.48 ± 0.38
FC (wt%)	17.85 ± 0.83
Ash (wt%)	4.40 ± 0.20
HHV (MJ/kg)	13.70 ± 0.20
CH_2Cl_2 extractives (wt%)	1.70 ± 0.01
Acid soluble lignin (wt%)	3.30 ± 0.51
Klason lignin (wt%)	14.32 ± 0.10
Total lignin (wt%)	17.62 ± 0.62
C (wt%)	34.00 ± 0.30
N (wt%)	2.50 ± 0.03
Protein (N * 6.25) (wt%)	15.62 ± 0.16
Glucan (wt%)	43.57 ± 2.80
Xylan (wt%)	20.10 ± 1.40
Galactan (wt%)	3.10 ± 0.50
Arabinan (wt%)	6.30 ± 0.30
Total Neutral sugar (wt%)	73.07 ± 5.00

The fatty acid profile of DS was determined as FAME derivatives and given in Table 3. The fatty acids were from C_{12} (lauric acid) to C_{24} (lignoceric acid) with the most abundant being palmitic acid (94 mg/g extract), followed by linoleic (27 mg/g extract) and oleic (19 mg/g extract) acids. Garton [37] found fatty acids from C_{14} to C_{22} in cocksfoot and rye grasses, while Mir et al. [35] found only palmitic, linolenic, oleic, and stearic acids in three forage grasses.

The XRD analysis of DS (Fig. 1a) showed a typical diffractogram of cellulose I with 2θ peaks at 15° and 22°, which were assigned to the planes of (101) and (002), respectively [21]. The CCI was determined as 0.375, and it is slightly higher than that reported for Napier grass (0.327) [36]. The sharp peak at 26.8° was assigned to quartz (silica) [38,39]. This same trend has been observed in the literature [40]. The peak at 28.5° was tentatively assigned to sylvite [41].

The FTIR spectroscopy was used to obtain nondestructive chemical information on DS (Fig. 1b). The infrared band assignments outlined in Refs. [29,42] were used for peak identification. A broadband around 3300 cm^{-1} was assigned to O–H stretching in polysaccharides and lignin. The band around 2919 cm^{-1} was assigned to C–H stretching from aliphatic structures, while the carbonyl absorption band around 1740 cm^{-1} was assigned to acetyl and uronic acid groups in xylan. The presence of lignin was confirmed by the distinct bands at 1518 and 1604 cm^{-1} assigned to aromatic skeletal vibrations. The broadband centered around 1036 cm^{-1} was assigned to C–O stretching mainly due to cellulose, hemicellulose, and lignin.

The cellulose crystallinity is a key factor in the degradability of biomass. The cellulose structural information was determined from the TCI (crystallinity) and LOI (cellulose I) measurements as 0.73 and 1.03, respectively. These were different from the values noted for Napier grass (TCI - 1.25 and LOI - 0.53) [36]. In addition, the LOI obtained in this study for DS was higher relative to sorghum residue (LOI - 0.75) [29]. The S/G ratio significantly influences lignin properties, such as reactivity and glass transition temperature [43]. The lignin S/G ratio in DS was estimated as 1.1, which was comparable to agricultural straw soda lignin at 1.05 [43]. It is noteworthy that Sun et al. [44] reported S/G ratios of 0.92 for switchgrass and 1.1 for maize by Raman spectroscopy.

3.2. *Thermal decomposition characteristics of DS at different heating rates*

Fig. 2a and b presents the TG and DTG curves for the thermal decomposition of DS in N_2 and air atmospheres, respectively, at different heating rates. Table 4 gives the data on critical peak temperature and resultant residues in the thermal process.

The plots show that both inert and oxidative DS thermal degradation follows a similar trend. Generally, the thermal decomposition of lignocellulosic biomass involves dehydration (I), devolatilization (II), and char formation/solid decomposition (III) stages, as clearly depicted on the thermograms. In both scenarios, the first main DTG peak appears below 100 °C, which corresponds to less than 5% weight loss. This may be attributed to moisture evaporation. Next is a barely visible shoulder at around 230 °C, and it is traditionally assigned to hemicellulose decomposition [45]. It is noteworthy, however, that the imperceptibility of this peak could be as a result of the overlapping of the thermal degradation of hemicellulose and cellulose components. This is closely followed by the highest peak in the thermal process at a temperature between 270 and 360 °C. Whereas some consider this a representation of the simultaneous decomposition of hemicellulose, cellulose and lignin constituents [11,31], others view it as an indication of cellulose degradation mainly [45]. The latter view is supported by the assertion that at temperatures above 250 °C, cellulose completely degrades in a rapid manner leading primarily to char formation [46]. It is noteworthy, however, that stage II represents a significant region, where hemicellulose and cellulose are predominantly degraded. Before the maximum peak, between 140 and 210 °C, a weight loss of less than 1% is observed. This may be due to the liberation of some low-molecular organics that are easily degradable [47]. A minor peak emerges at the wake of the decomposition trail around 600 °C. It has been reported that this may be indicative of the decomposition of lignin strongest bonds and/or thermal cracking of some residual organic compounds formed from the previous primary reactions [29,31]. Onsree et al. [4] essentially reported a similar trend in terms of the stages of decomposition at different temperature regimes. The temperature variation observed may be due to the fact that the thermal decomposition process was done in a macro TGA. Significantly, the thermograms for both N_2 and air atmospheres reveal a marginal variation in the residual weight with respect to the heating rate (Table 4) - a pointer to the fact that the weight loss trend is largely independent of the heating rate.

Furthermore, as the heating rate increases, the weight loss rate peaks shift to higher temperature as well as increase in height in absolute terms. For example, for the maximum peak, under N_2, the peak temperatures (height), and the heating rate, respectively are

Table 3
Fatty acid profile of *Digitaria sanguinalis* extract.

FAME	RT (min)	M^+ (*m/z*)	DS (mg/g extract)
Lauric acid (C12:0)	24.15	214	2.80
Myristic (C14:0)	28.69	242	3.10
Pentadecanoic acid (C15:0)	30.79	256	2.99
Palmitelaidic acid (16:1)	32.31	268	7.67
Palmitic acid (C16:0)	32.83	270	93.5
Heptadecanoic acid (C17:0)	34.83	284	6.65
Linoleic acid (C18:2)	35.84	294	27.2
Oleic acid (C18:1)	36.00	296	18.9
Stearic acid (C18:0)	36.54	298	9.26
Arachidic acid (C20:0)	40.00	326	7.78
Behenic acid (C22:0)	43.14	354	16.5
Tricosanoic acid (C23:0)	44.82	368	3.23
Lignoceric acid (C24:0)	46.85	382	12.8

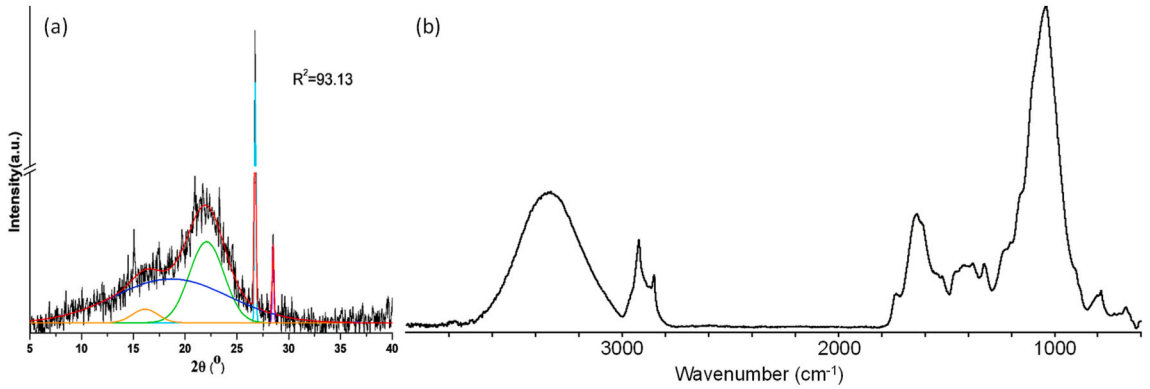

Fig. 1. (a) X-ray diffractogram and (b) FTIR spectrum of *Digitaria sanguinalis*.

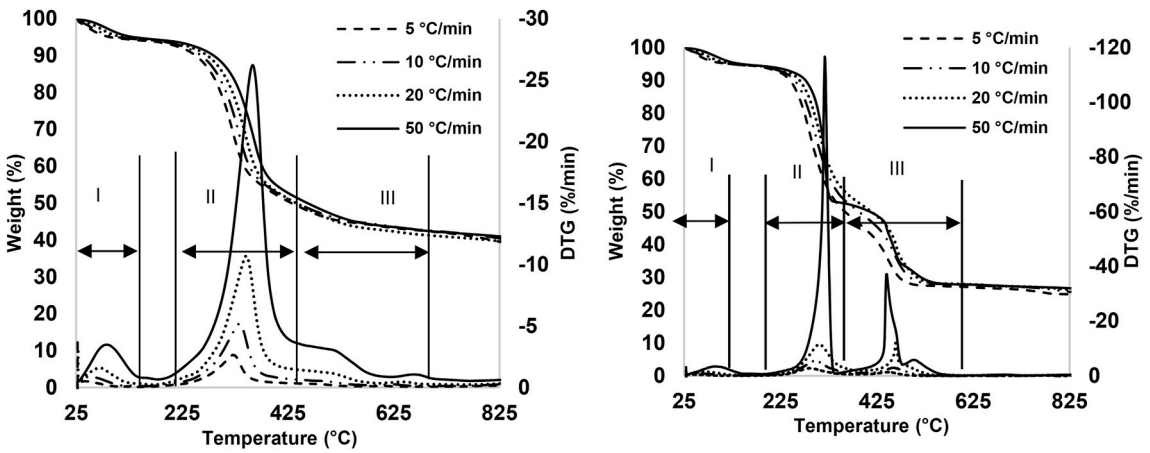

Fig. 2. Plots of thermal decomposition of DS in (a) N_2 and (b) air atmospheres.

Table 4
Thermal characteristics of DS decomposition under N_2 and air atmospheres.

	N_2			Air		
β (°C min^{-1})	T_p (°C)	DTG (%/min)	W_f (%)	T_p (°C)	DTG (%/min)	W_f (%)
5	43.6	−0.52	38.1	57.2	−0.46	24.6
	321.9	−2.64		285.3	−2.80	
				447.0	−1.35	
	608.5	−0.12		625.3	−0.07	
10	51.7	−0.87	38.9	56.04	−0.83	25.3
	332.9	−5.15		295.5	−5.48	
				459.0	−2.96	
	623.1	−0.25		637.2	−0.12	
20	70.6	−1.58	38.0	71.9	−1.51	25.3
	345.9	−10.69		306.2	−11.48	
				465.0	−13.09	
	641.9	−0.46		658.6	−0.26	
50	82.5	−3.48	39.7	89.0	−3.45	26.0
	358.8	−26.22		316.8	−116.6	
				445.8	−37.2	
	663.3	−1.05		686.0	−0.46	
Average			38.7±0.7			25.3±0.5

321.9 °C (2.64%/min), 332.9 °C (5.15%/min), 345.9 °C (10.69%/min), 358.8 °C (26.22%/min) and 5, 10, 20, 50 °C min^{-1}. A probable explanation could be that the rapid rates that characterize higher heating rates lead to heat transfer limitations and cause high thermal gradients within the DS sample; consequently, the decomposition temperature are pushed to higher values [47].

Specifically, the residual weight after thermal degradation for the air atmosphere (average of 25.3%) is comparatively less than that of N_2 (average of 38.7%). This is in agreement with findings from published literature [47]. It should be noted that the air atmosphere is an oxidative environment (combustion) with a relatively higher rate of reaction. Therefore, a higher decomposition rate is not

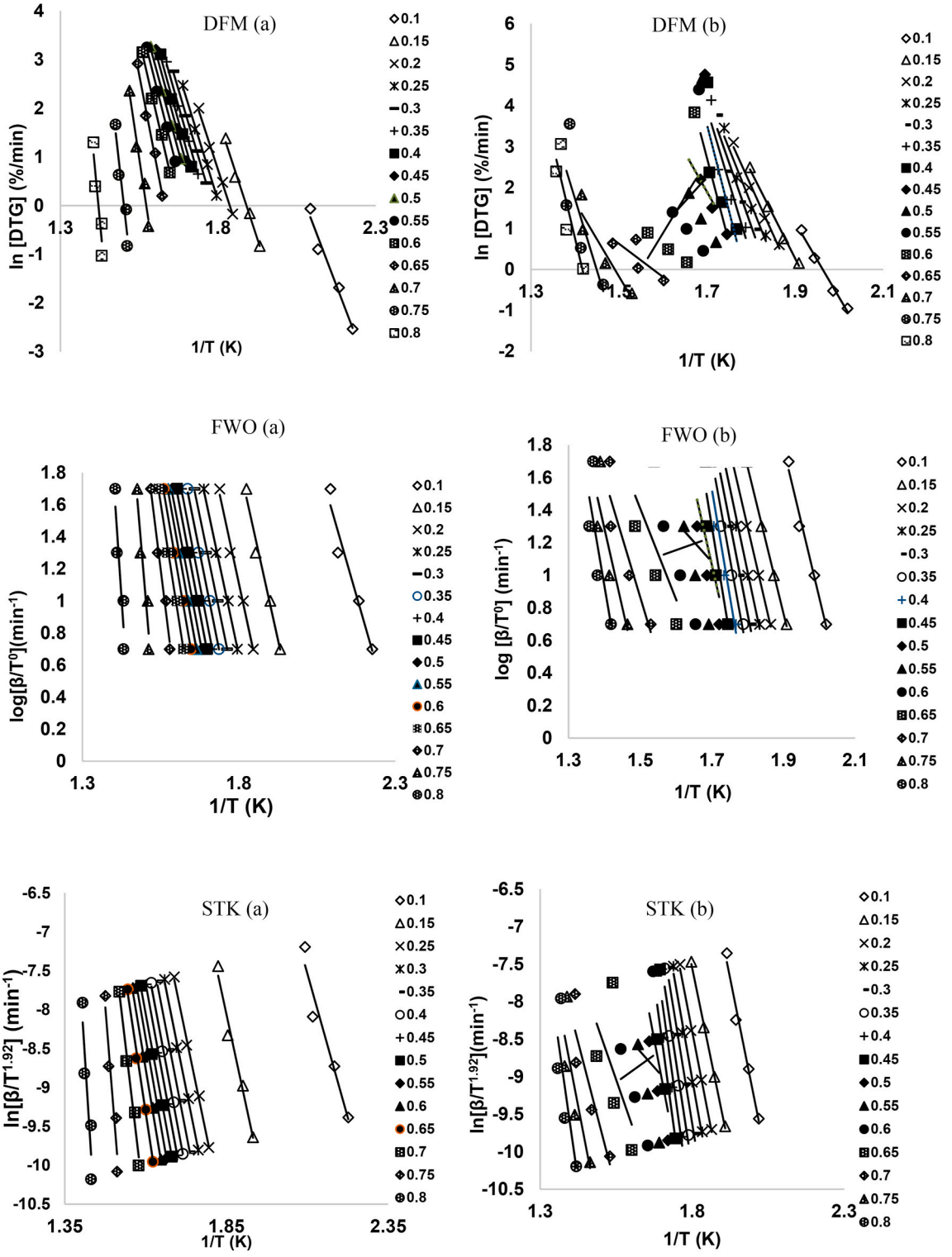

Fig. 3. Plots of linear curves for DFM, FWO, STK models in (a) N_2 and (b) air environments.

unexpected. Furthermore, it is observed that there was a minimal variation in the peak temperature, T_p, for the corresponding stages of degradation for both scenarios except for the maximum decomposition stage at 50 °C min^{-1}. At this heating rate, the DTG peak for air and N_2 environments respectively reads −116.6 and −26.22%/min. Notably, under air, a prominent peak protrudes at about 450 °C as against a shoulder under N2. This agrees with published data [14]. These observations could suggest a thermal degradation phenomenon that is related to the combustion of char residues because it has been opined that char formation is predominant in the latter stage of oxidative degradation processes [11,48].

3.3. Kinetic modeling

3.3.1. Model-free technique

The linear curves obtained by the application of DFM, FWO, and STK models under inert and airflow conditions, respectively, are depicted in Fig. 3a and b. The plot was restricted to a conversion ratio, α, ($0.1 \leq \alpha \leq 0.8$) because it spans the region where chemical reactions are predominant, and kinetic models are more likely to provide good approximations. It is shown that the application of the isoconversional models to the data of the inert environment has a strong correlation nearly over the entire conversion range with the coefficient of determination, $R2 > 0.9$, for a conversion ratio of 0.1–0.7. On the contrary, there was poor correlation mid-way into the conversion (above $\alpha > 0.4$) for the oxidizing environment so that the models provide good approximations only for the first half of the conversion. There have been a couple of reasons adduced for the parallel nature or otherwise of the linear plots. Alvarenga et al. [49] noted that the non-parallelism exhibited in the kinetic study suggests a change in the reaction mechanism at higher decomposition temperature. It was also observed that poor correlations of the linear plots may be due to the heterogeneous character the solid assumes at the latter stages of decomposition [50]. The reaction mechanism at this stage involves a complex interplay of secondary reactions, diffusion, and in-situ catalysis of metals.

Fig. 4a and b shows the variation of apparent activation energy, E_α, with conversion ratio, α, for the three isoconversional methods. Similarly, Table 5 shows the E_α, α, and coefficient of determination, R^2 data. The α is within the limits of 0.1–0.8 with an increment of 0.05. There is an apparent distinction between the trend shown for the inert and oxidative conditions. In the inert situation, the three methods show closely similar trends particularly the FWO and STK, which were based on the temperature integral approximation in the kinetic rate model. On the other hand, DFM is a differential method that is devoid of the oversimplified integral approximation of the temperature function, and relatively, it is expected to be more accurate [28]. The profile of the E_α could be delineated into three different stages. The early stage of decomposition, $\alpha = 0.1–0.2$, for FDM, FWO, and STK presents average values of E_α as 157 kJ/mol, 149 kJ/mol, and 149 kJ/mol respectively. Next the average values of E_α were computed as 197 kJ/mol, 185 kJ/mol, and 185 kJ/mol for $\alpha = 0.25–0.6$ for the models according to the earlier order. In the final reaction stage ($\alpha = 0.65–0.8$), the E_α spiked to much higher levels presenting average values for the models as 422 kJ/mol, 366 kJ/mol, and 374 kJ/mol. The decomposition of DS involves multi-step reactions of the polymeric constituents leading to a distribution of the activation energies [28]. Thus, underscoring the dependency of activation energy on conversion. The activation energy refers to the minimum energy barrier that must be overcome for a reaction to occur to ensure the formation of new products. The higher E_α values at the latter stage of the conversion process suggest that the initiation of reactions was relatively more difficult. The E_α trend shown here for the inert environment agrees well with trends reported in literature for corn stalk (148–473 kJ/mol) [28], and tobacco waste (144–338 kJ/mol) [12].

The E_α profile for the airflow environment, on the other hand, is distinctively different as it presents a curve with a wavy pattern having a deep valley mid-way into the conversion. A similar trend has been observed in literature [12]. It is noteworthy that the values of E_α in the early stages, $\alpha = 0.1–0.2$, relative to the inert conditions were slightly higher. A similar observation was made in published literature in which the values of Eα at the first stage for synthetic air and N_2 atmosphere were determined to be 200 and 133 kJ/mol, respectively [26]. A plausible reason is the exothermic reactions that characterize the oxidation of the volatiles liberated. This leads to

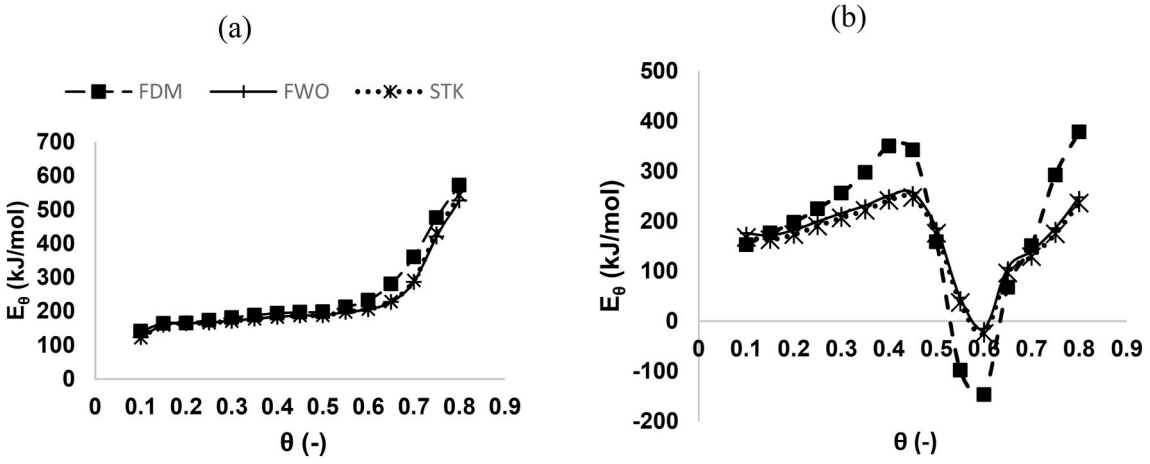

Fig. 4. Plots of apparent activation energy, E_α, against conversion ratio, α, (a) N_2 and (b) air environments.

Table 5
Values of E_α (kJ/mol), and R^2 for DFM, FWO, STK models under N_2 and air environments.

	α	N_2						Air					
		DFM		FWO		STK		DFM		FWO		STK	
		E_α (kJ/mol)	R^2	E_α(kJ/mol)	R^2	E_α(kJ/mol)	R^2	E_α(kJ/mol)	R^2	E_α(kJ/mol)	R^2	E_α(kJ/mol)	R^2
STAGE I	0.1	141.3	0.969	123.4	0.951	122.3	0.942	152.4	0.988	175.8	0.986	167.6	0.982
	0.15	164.4	0.990	160.2	0.982	159.9	0.978	176.2	0.995	171.6	1.000	162.8	0.999
	0.2	165.4	0.995	164.6	0.991	164.2	0.989	197.4	0.986	182.0	0.998	173.1	0.996
Average		157.0±11.1		149.4±18.5		148.8±18.8		175.3±18.3		176.5±4.3		167.8±4.2	
STAGE II	0.25	173.6	0.997	166.8	0.996	166.2	0.996	224.7	0.966	199.2	0.992	190.1	0.988
	0.3	181.3	0.997	171.9	0.997	171.4	0.996	255.9	0.927	215.7	0.977	206.5	0.971
	0.35	188.8	0.997	178.3	0.996	178.0	0.995	297.2	0.855	230.9	0.955	221.6	0.47
	0.4	194.2	0.997	183.3	0.997	183.2	0.996	349.9	0.682	250.7	0.880	241.3	0.869
	0.45	197.2	0.996	187.6	0.997	187.6	0.995	342.3	0.404	256.9	0.685	247.4	0.671
	0.5	198.7	0.997	188.3	0.998	188.2	0.996	158.5	0.073	185.4	0.319	175.9	0.304
	0.55	212.9	0.998	198.0	0.997	198.3	0.996	−98.3	0.04	46.9	0.032	37.3	0.021
	0.6	232.6	0.996	205.9	0.996	206.6	0.995	−147.0	0.249	−14.9	0.006	−24.8	0.020
Average		197.4±17.3		185.0±12.1		184.9±12.5		172.9±180.7		171.4±93.7		161.9±93.9	
STAGE III	0.65	280.7	0.991	227.3	0.994	228.9	0.992	67.6	0.642	106.7	0.365	96.3	0.336
	0.7	360.6	0.974	286.6	0.981	291.1	0.980	150.9	0.879	140.0	0.854	129.1	0.828
	0.75	476.5	0.915	420.7	0.922	431.7	0.918	292.1	0.621	185.8	0.740	174.5	0.714
	0.8	572.1	0.877	527.5	0.861	543.4	0.855	378.2	0.773	247.7	0.647	236.0	0.628
Average		422.5±111.0		365.5±116.8		373.8±122.4		222.2±120.6		170.1±52.9		159.0±52.4	

an increase in the reaction rate, and consequently, an increase in the energy barrier [26]. The next stage consists of two parts: (1) between $\alpha = 0.25–0.45$ the E_α rises from 224.7, 199.2, and 190.1 kJ/mol, and hits 342.3, 256.9, and 247.4 kJ/mol, respectively for the isoconversional methods; (2) between $\alpha = 0.5–0.6$ the values of E_α plummets deeply even to negative values. This is not unusual since this is an intricate thermal process that is not species-specific. These activation energy values are "apparent" and can therefore show marked deviations from the intrinsic kinetic parameters of an individual step [51]. In the final decomposition stage, a sharp slope is seen in which the values of E_α reach another peak (378.2, 247.7, and 236.0 kJ/mol) for DFM, FWO, STK models, respectively. It is noteworthy that the average values of E_α for the last two stages under air scenarios relative to N_2 are lower. The markedly different trend displayed in the last two stages may be suggestive of dissimilar reaction mechanisms and complex degradation phenomena. It has been noted that whereas the latter decomposition stage of oxidative processes consists of char burnout, the inert thermal decomposition processes experience char formation [15]. It is important to note that the trend above underscores the fact that pyrolytic and oxidative processes involve complex multi-step reaction mechanisms.

3.3.2. Model-fitting technique

The values of E_α, A, and R^2 for both N_2 and air atmospheres, obtained using the CR model, are shown in Table 6. These were deduced according to Eq. (5) from the slope of plots of $\ln\left(\frac{g(\alpha)}{T^2}\right)$ against $\frac{1}{T}$ for different heating rates. In deploying the integral chemical reaction model, the reaction order, *n*, could be a positive or negative integer, however, the value of *n* was restricted, as shown in Eq. (9) [52].

$$0 \leq n \leq 3 \tag{9}$$

The E_α for the second-order reaction model ranges from 118 to 135 kJ/mol and 100–255 kJ/mol for N_2 and air conditions, respectively. In both thermal conditions, the diffusional model presents the highest average value of 139 kJ/mol (N_2) and 149 kJ/mol (air), which represents the closest to the average value E_α (190 kJ/mol; N_2) and (167 kJ/mol; air) of the integral model-free techniques for stage II. This implies that diffusion plays a critical role in this decomposition stage for the tropical grass being investigated. It has been explained that where mobility of reactant constituents depends on lattice defects, solid-state reactions mostly transpire between either the crystal lattices or the molecules penetrating the lattices [52]. For this investigation, the reaction models shown in Table 1 were tested for the best fit in the CR technique at the three stages earlier identified under the model-free kinetic study. Several researchers have opined that comparing the average value of E_α obtained from different heating rates with that of a model-free technique such as FWO can be used in the selection of a suitable reaction mechanism [11,52]. They postulated that the closest Eα among the given integral models represents a probable mechanism. In the present study, this postulation was employed. Furthermore, due to a couple of non-realistic values obtained for some models at some stages of decomposition, consideration was given to the values of E_α that have the same order of magnitude as the model-free kinetic data. From the foregoing, it is only the data from stage II that satisfy this criterion, and are presented for discussion in Table 6. The chemical reaction and diffusional models represent the possible reaction mechanisms that govern the thermal decomposition process in both inert and oxidative environments. It is shown that regardless of the integral model, the activation energy and pre-frequency exponential factor increase with an increase in heating rates, and for the chemical reaction model, reaction order.

4. Conclusion

A tropical grass species (*Digitaria sanguinalis*) obtained from Nigeria was subjected to thermal decomposition under inert and oxidative atmospheres. The model-free and model-fitting techniques were used in the investigation of the kinetic data of the grass. Before this, the grass sample was submitted to thermal, structural, and physico-chemical characterization techniques, through thermogravimetry, spectroscopic analyses, and wet-chemistry methods, respectively. This comparative study is part of a larger project on the investigation of a couple of grass species as potential energy crops both for pyrolytic and combustion applications within the context of a local environment. The grass sample showed clear physico-chemical and structural variations relative to some grasses from previous studies. The elemental analysis showed that in the DS sample 34% C, 2.5% N, and 4.4% ash were present. The total crystallinity index and lateral order index, respectively, were estimated as 0.73 and 1.03. The fatty acids detected ranged from C_{12} (lauric acid) to C_{24} (lignoceric acid).

Regarding the thermal decomposition, the derivative weight loss reveals a distinct variation in the decomposition behavior of the biomass in the thermal atmospheres explored such that at 50 °C/min^{-1} the weight loss rate peak for N_2 and air atmospheres read −26.22 and −116.6%/min, respectively. In the latter stages of decomposition in air, around 450 °C, a prominent peak emerges that is suggestive of a unique degradation phenomenon (combustion). In addition, whereas the isoconversional methods presented a strong correlation for almost the entire conversion range in N_2, they provided a good approximation for just the first half of the conversion in air. The model-fitting method suggests that chemical reaction and diffusional models play dominant roles in the thermal decomposition of the tropical grass, whether in an inert or an oxidative environment. It was thus concluded that the thermal degradation of the biomass in question proceeded mainly as complex multi-step reaction mechanisms. The grass species investigated have shown a huge potential for bioenergy applications. The kinetic data would also contribute significantly to the development of the associated thermochemical processes and the design and optimization of reactors/combustors.

Table 6
Values of E_α (kJ/mol), R^2, A (min^{-1}) for inert and airflow conditions (stage II) based on Coats-Redfern (CR) model.

Inert	5 °C min^{-1}			10 °C min^{-1}			20 °C min^{-1}			50 °C min^{-1}			Average		
$g(\alpha)$	E_α	R^2	A	E_α	R^2	A	E_α	R^2	A	E_α	R^2	A	E_α	R^2	A
Chemical reaction model															
$(1-(1-\alpha))^{-1}/(-1)$	95.3	0.993	4.8E09	97.5	0.991	1.1E10	102.6	0.991	4.6E10	108.6	0.990	2.7E11	101.0	0.991	8.2E10
$(1-(1-\alpha))^{-2}/(-2)$	118.0	0.987	8.8E11	120.7	0.984	2.2E12	127.1	0.984	1.0E13	134.5	0.983	7.1E13	125.1	0.985	2.1E13
Diffusional model															
α^2	110.1	0.999	2.7E10	112.9	0.999	6.8E10	118.8	0.999	3.0E11	125.8	0.999	2.0E12	116.9	0.999	6.0E11
$(1-\alpha)*\ln(1-\alpha)+\alpha$	119.7	0.999	1.3E11	122.7	0.999	3.2E11	129.1	0.999	1.5E12	136.8	0.999	1.1E13	127.07	0.999	3.2E12
$(1-(1-\alpha)^{1/3})^2$	130.7	0.998	3.5E11	133.9	0.998	9.1E11	141.0	0.997	4.6E12	149.4	0.997	3.7E13	138.7	0.998	1.1E13
$1-(2/3)\alpha-(1-\alpha)^{2/3}$	123.4	0.999	6.5E10	126.4	0.998	1.7E11	133.1	0.998	8.1E11	141.0	0.998	6.0E12	130.9	0.998	1.8E12
Airflow															
Chemical reaction model															
$(1-(1-\alpha))^{-1}/(-1)$	80.5	0.989	2.6E08	77.3	0.983	1.9E08	72.8	0.962	1.2E08	203.8	0.982	4.0E20	108.6	0.979	10.0E19
$(1-(1-\alpha))^{-2}/(-2)$	99.8	0.994	2.7E10	95.8	0.989	1.5E10	90.3	0.970	6.8E09	255.0	0.975	2.5E25	135.2	0.982	6.2E24
Diffusional model															
α^2	91.3	0.966	6.7E08	87.4	0.957	4.0E08	81,8	0.927	1.8E08	237.9	0.992	1.1E23	124.6	0.961	2.9E22
$(1-\alpha)*\ln(1-\alpha)+\alpha$	99.3	0.970	2.4E09	95.1	0.962	1.3E09	89.0	0.932	5.1E08	259.6	0.991	6.2E24	135.7	0.964	1.6E24
$(1-(1-\alpha)^{1/3})^2$	108.7	0.975	4.9E09	104.0	0.966	2.4E09	97.3	0.938	8.0E08	284.4	0.990	3.0E26	148.6	0.967	7.4E25
$1-(2/3)\alpha-(1-\alpha)^{2/3}$	102.4	0.972	1.1E09	98.0	0.963	5.8E08	91.8	0.934	2.2E08	267.8	0.991	8.2E24	140.0	0.965	2.1E24

Authors statement

Manuscript title: Physicochemical characterization, thermal decomposition and kinetic modeling of Digitaria sanguinalis under nitrogen and air environments All persons who meet authorship criteria are listed as authors, and all authors certify that they have participated sufficiently in the work to take public responsibility for the content, including participation in the concept, design, analysis, writing, or revision of the manuscript. Furthermore, each author certifies that this manuscript has not been, and will not be submitted to or published in any other publication before its appearance in Case Studies in Thermal Engineering.

Declaration of competing interest

The authors declare that they have no known competing financial interests or personal relationships that could have appeared to influence the work reported in this paper.

Acknowledgement

None.

Appendix A. Supplementary data

Supplementary data to this article can be found online at https://doi.org/10.1016/j.csite.2021.101138.

Funding

This research did not receive any specific grant from funding agencies in the public, commercial, or not-for-profit sectors.

References

[1] A. Elorf, B. Sarh, Excess air ratio effects on flow and combustion caracteristics of pulverized biomass (olive cake), Case Stud. Therm. Eng. 13 (2019) 1–11, https://doi.org/10.1016/j.csite.2018.100367.
[2] A.A. Adeleke, J.K. Odusote, O.A. Lasode, P.P. Ikubanni, M. Malathi, D. Paswan, Mild pyrolytic treatment of gmelina arborea for optimum energetic yields, Cogent Eng 6 (2019) 1–13.
[3] J.O. Ogunkanmi, D.M. Kulla, N.O. Omisanya, M. Sumaila, D.O. Obada, D. Dodoo-Arhin, Extraction of bio-oil during pyrolysis of locally sourced palm kernel shells: effect of process parameters, Case Stud. Therm. Eng. 12 (2018) 711–716, https://doi.org/10.1016/j.csite.2018.09.003.
[4] T. Onsree, N. Tippayawong, A. Zheng, H. Li, Pyrolysis behavior and kinetics of corn residue pellets and eucalyptus wood chips in a macro thermogravimetric analyzer, Case Stud. Therm. Eng. 12 (2018) 546–556, https://doi.org/10.1016/j.csite.2018.07.011.
[5] S.S.V. Varsha, A.K. Vuppaladadiyam, F. Shehzad, H. Ghaedi, S. Murugavelh, W. Dong, E. Antunes, Co-pyrolysis of microalgae and municipal solid waste: a thermogravimetric study to discern synergy during co-pyrolysis process, J. Energy Inst. 94 (2021) 29–38, https://doi.org/10.1016/j.joei.2020.10.010.
[6] S. Hidayat, M.S. Abu Bakar, Y. Yang, N. Phusunti, A.V. Bridgwater, Characterisation and Py-GC/MS analysis of Imperata Cylindrica as potential biomass for bio-oil production in Brunei Darussalam, J. Anal. Appl. Pyrolysis 134 (2018) 510–519, https://doi.org/10.1016/j.jaap.2018.07.018.
[7] A. Ngom, M.S. Mbaye, A.A. Camara, M. Gueye, K. Noba, Grasses (Poaceae) from Senegal: new records checklist, biogeographical affinities and biological types, Eur. Sci. J. ESJ. 16 (2020) 177–187, https://doi.org/10.19044/esj.2020.v16n18p177.
[8] A.M. Tilley, H.L. Walker, Evaluation of Curvularia intermedia (Cochliobolus intermedius) as a potential microbial herbicide for large crabgrass (Digitaria sanguinalis), Biol. Contr. 25 (2002) 12–21.
[9] N. Rassai, N. Boutammachte, H. El Hassani, A. Almers, E.M. Boudi, A. Bekraoui, Effect of the particle size of pulverized olive cake on combustion parameters in Stirling engine in Morocco, Case Stud. Therm. Eng. 12 (2018) 433–444, https://doi.org/10.1016/j.csite.2018.06.004.
[10] A.A. Adeleke, J.K. Odusote, P.P. Ikubanni, O.A. Lasode, M. Malathi, D. Paswan, The ignitability, fuel ratio and ash fusion temperatures of torrefied woody biomass, Heliyon 6 (2020), https://doi.org/10.1016/j.heliyon.2020.e03582, 1-7.
[11] R. Chen, Q. Li, X. Xu, D. Zhang, R. Hao, Combustion characteristics, kinetics and thermodynamics of Pinus Sylvestris pine needle via non-isothermal thermogravimetry coupled with model-free and model-fitting methods, Case Stud. Therm. Eng. 22 (2020) 100756, https://doi.org/10.1016/j.csite.2020.100756.
[12] W. Wu, Y. Mei, L. Zhang, R. Liu, J. Cai, Kinetics and reaction chemistry of pyrolysis and combustion of tobacco waste, Fuel 156 (2015) 71–80, https://doi.org/10.1016/j.fuel.2015.04.016.
[13] M. Wilk, A. Magdziarz, M. Gajek, M. Zajemska, K. Jayaraman, Combustion and kinetic parameters estimation of torrefied pine, acacia and Miscanthus giganteus using experimental and modelling techniques, Bioresour. Technol. 243 (2017) 304–314, https://doi.org/10.1016/j.biortech.2017.06.116.
[14] A. Mlonka-m, A. Magdziarz, T. Dziok, W. Nowak, Laboratory studies on the in fl uence of biomass particle size on pyrolysis and combustion using TG GC/MS, Fuel 252 (2019) 635–645, https://doi.org/10.1016/j.fuel.2019.04.091.
[15] Z. Xu, X. Xiao, P. Fang, L. Ye, J. Huang, H. Wu, Z. Tang, D. Chen, Comparison of combustion and pyrolysis behavior of the peanut shells in air and N2: kinetics, thermodynamics and gas emissions, Sustainability 12 (2020), https://doi.org/10.3390/su12020464.
[16] S. Hameed, A. Sharma, V. Pareek, H. Wu, Y. Yu, A review on biomass pyrolysis models : kinetic , network and mechanistic models, Biomass Bioenergy 123 (2019) 104–122, https://doi.org/10.1016/j.biombioe.2019.02.008.
[17] A.A. Adeleke, J.K. Odusote, O.A. Lasode, P. Ikubanni, M. Madhurai, D. Paswan, Evaluation of thermal decomposition characteristics and kinetic parameters for gmelina wood, Biofuels 10 (2019) 1–7.
[18] E. Karampinis, D. Vamvuka, S. Sfakiotakis, P. Grammelis, G. Itskos, E. Kakaras, Comparative study of combustion properties of five energy crops and Greek lignite, Energy and Fuels 26 (2012) 869–878, https://doi.org/10.1021/ef2014088.
[19] Y.D. Singh, P. Mahanta, U. Bora, Comprehensive characterization of lignocellulosic biomass through proximate, ultimate and compositional analysis for bioenergy production, Renew. Energy 103 (2017) 490–500, https://doi.org/10.1016/j.renene.2016.11.039.
[20] F.C.R. Lopes, J.C. Pereira, K. Tannous, Thermal decomposition kinetics of guarana seed residue through thermogravimetric analysis under inert and oxidizing atmospheres, Bioresour. Technol. 270 (2018) 294–302, https://doi.org/10.1016/j.biortech.2018.09.021.

[21] A.O. Balogun, F. Sotoudehniakarani, A.G. Mcdonald, Thermo-kinetic, spectroscopic study of brewer's spent grains and characterisation of their pyrolysis products, J. Anal. Appl. Pyrolysis 127 (2017) 8–16, https://doi.org/10.1016/j.jaap.2017.09.009.
[22] M. Almazrouei, I. Janajreh, Model-fitting approach to kinetic analysis of non-isothermal pyrolysis of pure and crude glycerol, Renew. Energy 145 (2020) 1693–1708, https://doi.org/10.1016/j.renene.2019.07.095.
[23] M.S. Masnadi, R. Habibi, J. Kopyscinski, J.M. Hill, X. Bi, C.J. Lim, N. Ellis, J.R. Grace, Fuel characterization and co-pyrolysis kinetics of biomass and fossil fuels, Fuel 117 (2014) 1204–1214, https://doi.org/10.1016/j.fuel.2013.02.006.
[24] A.O. Balogun, O.A. Lasode, A.G. McDonald, Devolatilisation kinetics and pyrolytic analyses of Tectona grandis (teak), Bioresour. Technol. 156 (2014), https://doi.org/10.1016/j.biortech.2014.01.007.
[25] A.O. Balogun, A.G. McDonald, Decomposition kinetic study, spectroscopic and pyrolytic analyses of Isoberlinia doka and Pinus ponderosa, Biomass Convers. Biorefinery. 6 (2016), https://doi.org/10.1007/s13399-015-0185-3.
[26] Y.J. Rueda-Ordóñez, K. Tannous, Drying and thermal decomposition kinetics of sugarcane straw by nonisothermal thermogravimetric analysis, Bioresour. Technol. 264 (2018) 131–139, https://doi.org/10.1016/j.biortech.2018.04.064.
[27] A. Ashraf, H. Sattar, S. Munir, R. Husk, A comparative applicability study of model-fitting and model-free kinetic analysis approaches to non-isothermal pyrolysis of coal and agricultural residues, Fuel 240 (2019) 326–333, https://doi.org/10.1016/j.fuel.2018.11.149.
[28] J. Cai, D. Xu, Z. Dong, X. Yu, Y. Yang, S.W. Banks, A. V Bridgwater, Processing thermogravimetric analysis data for isoconversional kinetic analysis of lignocellulosic biomass pyrolysis : case study of corn stalk, Renew. Sustain. Energy Rev. 82 (2018) 2705–2715, https://doi.org/10.1016/j.rser.2017.09.113.
[29] A.O. Balogun, O.A. Lasode, H. Li, A.G. McDonald, Fourier transform infrared (FTIR) study and thermal decomposition kinetics of sorghum bicolour glume and albizia pedicellaris residues, Waste and Biomass Valorization 6 (2014), https://doi.org/10.1007/s12649-014-9318-3.
[30] H. Haykırı-açma, S. Yaman, Kinetic modelling of RDF pyrolysis : model-fitting and model-free approaches, Waste Manag. 48 (2016) 275–284, https://doi.org/10.1016/j.wasman.2015.11.027.
[31] C.N. Arenas, M.V. Navarro, J.D. Martínez, Pyrolysis kinetics of biomass wastes using isoconversional methods and the distributed activation energy model, Bioresour. Technol. 288 (2019) 1–11, https://doi.org/10.1016/j.biortech.2019.121485.
[32] J.I. Sultan, H.A.Q. Nawaz, M. Yaqoob, Nutritive value of marginal land grasses of northern grasslands of Pakistan, Pakistan J. Bot. 39 (2007) 1071–1082.
[33] I.D. Lee, H.S. Lee, Digitaria chemical composition_Lee1999.pdf, J. Korean Grassl. Sci. 19 (1999) 197–202.
[34] I.Y. Mohammed, Y.A. Abakr, F.K. Kazi, S. Yusup, I. Alshareef, S.A. Chin, Comprehensive characterization of napier grass as a feedstock for thermochemical conversion, Energies 8 (2015) 3403–3417, https://doi.org/10.3390/en8053403.
[35] P.S. Mir, S. Bittman, D. Hunt, T. Entz, B. Yip, Lipid content and fatty acid composition of grasses sampled on different dates through the early part of the growing season, Can. J. Anim. Sci. 86 (2006) 279–290, https://doi.org/10.4141/A05-050.
[36] A. Luengnaruemitchai, C. Anupapwisetkul, Surface morphology and cellulose structure of Napier grass pretreated with the ionic liquid 1-ethyl-3-methylimidazolium acetate combined with either water or dimethyl sulfoxide as a co-solvent under microwave irradiation, Biomass Convers. Biorefinery 10 (2020) 435–446, https://doi.org/10.1007/s13399-019-00422-4.
[37] G.A. Garton, Fatty acid composition of the lipids of pasture grasses, Nature 187 (1960) 511–512.
[38] J. Chisholm, Comparison of quartz standards for X-ray difraction analysis: HSE A9950 (Sikron F600) and NIST SRM 1878, Ann. Occup. Hyg. 49 (2005) 351–358.
[39] P.P. Ikubanni, M. Oki, A.A. Adeleke, A.A. Adediran, O.S. Adesina, Influence of temperature on the chemical compositions and microstructural changes of ash formed from palm kernel shell, Results Eng 8 (2020) 1–9.
[40] A.G. Sangster, Characteristics of silica deposition in Digitaria sanguinalis (L.) scop. (Crabgrass), Ann. Bot. 41 (1977) 341–350, https://doi.org/10.1093/oxfordjournals.aob.a085296.
[41] S. Martínez-Ramírez, M. Frías, E.Y. Nakanishi, H. Savastano, Pozzolanic reaction of a biomass waste as mineral addition to cement based materials: studies by nuclear magnetic resonance (NMR), Int. J. Concr. Struct. Mater. 13 (2019) 1–8, https://doi.org/10.1186/s40069-019-0342-3.
[42] A. Huang, Q. Zhou, J. Liu, B. Fei, S. Sun, Distinction of three wood species by Fourier transform infrared spectroscopy and two-dimensional correlation IR spectroscopy, J. Mol. Struct. 883–884 (2008) 160–166, https://doi.org/10.1016/j.molstruc.2007.11.061.
[43] H. Li, A.G. McDonald, Fractionation and characterization of industrial lignins, Ind. Crop. Prod. 62 (2014) 67–76, https://doi.org/10.1016/j.indcrop.2014.08.013.
[44] L. Sun, P. Varanasi, F. Yang, D. Loqué, B.A. Simmons, S. Singh, Rapid determination of syringyl: guaiacyl ratios using FT-Raman spectroscopy, Biotechnol. Bioeng. 109 (2012) 647–656, https://doi.org/10.1002/bit.24348.
[45] M. Gogoi, K. Konwar, N. Bhuyan, R. Chandra, Assessments of pyrolysis kinetics and mechanisms of biomass residues using thermogravimetry, Bioresour. Technol. Reports. 4 (2018) 40–49, https://doi.org/10.1016/j.biteb.2018.08.016.
[46] S. Gaur, T.B. Reed, Thermal Data for Natural and Sythentic Fuels, First, Marcel Dekker, New York, 1998. http://library1.nida.ac.th/termpaper6/sd/2554/19755.pdf.
[47] H. Sattar, I. Muzaffar, S. Munir, Thermal and kinetic study of rice husk, corn cobs, peanut crust and Khushab coal under inert (N2) and oxidative (dry air) atmospheres, Renew. Energy 149 (2020) 794–805, https://doi.org/10.1016/j.renene.2019.12.020.
[48] Y. Ding, B. Huang, C. Wu, Q. He, K. Lu, Kinetic model and parameters study of lignocellulosic biomass oxidative pyrolysis, Energy 181 (2019) 11–17, https://doi.org/10.1016/j.energy.2019.05.148.
[49] L.M. Alvarenga, T.P. Xavier, M.A.S. Barrozo, M.S. Bacelos, T.S. Lira, Analysis of reaction kinetics of carton packaging pyrolysis, Procedia Eng 42 (2012) 113–122, https://doi.org/10.1016/j.proeng.2012.07.401.
[50] X. Wang, M. Hu, W. Hu, Z. Chen, S. Liu, Z. Hu, B. Xiao, Thermogravimetric kinetic study of agricultural residue biomass pyrolysis based on combined kinetics, Bioresour. Technol. 219 (2016) 510–520, https://doi.org/10.1016/j.biortech.2016.07.136.
[51] S. Vyazovkin, A.K. Burnham, J.M. Criado, L.A. Pérez-Maqueda, C. Popescu, N. Sbirrazzuoli, ICTAC Kinetics Committee recommendations for performing kinetic computations on thermal analysis data, Thermochim. Acta 520 (2011) 1–19, https://doi.org/10.1016/j.tca.2011.03.034.
[52] Y. Ding, O.A. Ezekoye, S. Lu, C. Wang, R. Zhou, Comparative pyrolysis behaviors and reaction mechanisms of hardwood and softwood, Energy Convers. Manag. 132 (2017) 102–109, https://doi.org/10.1016/j.enconman.2016.11.016.